

# THE ASTROSPHERE OF THE ASYMPTOTIC GIANT BRANCH STAR IRC+10216

Raghvendra Sahai

*Jet Propulsion Laboratory, MS 183-900, California Institute of Technology, Pasadena, CA  
91109*

sahai@jpl.nasa.gov

and

Christopher K. Chronopoulos

*Space Sciences Laboratory, University of California, Berkeley, CA 94720*

## ABSTRACT

We have discovered a very extended shock structure (i.e., with a diameter of about  $24'$ ) surrounding the well-known carbon star IRC+10216 in ultraviolet images taken with the GALEX satellite. We conclude that this structure results from the interaction of IRC+10216's molecular wind with the interstellar medium (ISM), as it moves through the latter. All important structural features expected from theoretical models of such interactions are identified: the termination shock, the astrosheath, the astropause, the bowshock, and an astrotail (with vortices). The extent of the astropause provides new lower limits to the envelope age (69,000 years) and mass ( $1.4 M_{\odot}$ , for a mass-loss rate of  $2 \times 10^{-5} M_{\odot} \text{ yr}^{-1}$ ). From the termination-shock standoff distance, we find that IRC+10216 is moving at a speed of about  $\gtrsim 91 \text{ km s}^{-1} (1 \text{ cm}^{-3} / n_{\text{ISM}})^{1/2}$  through the local ISM.

*Subject headings:* stars: AGB and post-AGB, stars: mass-loss, stars: individual (IRC+10216), circumstellar matter, reflection nebulae

## 1. Introduction

The carbon-rich star IRC+10216 is the closest ( $D \sim 120 - 150$  pc) Asymptotic Giant Branch (AGB) star with a high mass loss rate ( $\dot{M} \sim 2 \times 10^{-5} M_{\odot} \text{ yr}^{-1}$ ) (e.g., Crosas & Menten 1997, Groenewegen, van der Veen, & Matthews 1998), and has been extensively observed from radio to optical wavelengths, and with a variety of imaging and spectroscopic techniques. These studies have led to a fairly comprehensive model of this object, consisting of a very cool ( $\gtrsim 2000$  K) star surrounded by a massive, extended, roughly spherical circumstellar envelope (CSE) expanding at  $14 \text{ km s}^{-1}$ . High spatial resolution imaging observations show that the envelope shows organized departures from spherical symmetry on the smallest scales, which are most likely a signature that the mechanism or mechanisms which transform the round CSEs of AGB stars into planetary nebulae (PNs) with a dazzling variety of shapes with non-spherical symmetries, have begun their operation in this object (Sahai 2009).

Studies of IRC+10216 over the years following its discovery have led to great progress in our understanding of the mass-loss process on the AGB, and hence the late evolution of intermediate mass stars and their role in the enrichment of the ISM with the products of CNO and  $3\text{-}\alpha$  nucleosynthesis as well as particulate matter. But both the progenitor mass of, and the total amount of matter ejected into the ISM by, IRC+10216, depend on the envelope's outer extent, which remains unknown. From the deepest imaging studies undertaken so far, the circumstellar envelope (CSE) has been traced out to a radius of  $\sim 200''$ , via dust scattering of Galactic starlight (Mauron & Huggins 2000, Leão et al. 2006). This radius corresponds to matter ejected from the star about  $8000(D/120 \text{ pc}) \text{ yr}$  ago.

In this Letter, we use deep GALEX images to trace the IRC+10216 CSE to its outer boundary, which has become visible as a result of the CSE's interaction with the ISM, presumably due to IRC+10216's motion through the latter. IRC+10216 is the first carbon-rich AGB star, and the third AGB star (after R Hya and Mira, which are oxygen-rich: Ueta et al. 2006, Martin et al. 2007) in which such an interaction has now been observed. We report on our analysis of the shape, size and structure of the CSE-ISM interaction observed in the GALEX images, provide new lower limits for the duration of heavy mass-loss and the total mass of ejecta in IRC+10216, and determine its motion through the ISM.

## 2. Observations & Results

We retrieved pipeline-calibrated FUV and NUV images of IRC+10216 from the GALEX archive; the bandpass (angular resolution) is 1344-1786 Å(4.5'') and 1771-2831 Å(6.0''), respectively, and the pixel size is 1.5'' × 1.5'' (Morrissey et al. 2005). The data were taken on 2008 Jan 15, each with an exposure time of 8782 sec. In Fig. 1a, we show a composite FUV/NUV image, and in Fig. 1b, the FUV image by itself. Field stars in each image have been removed using a customised IDL routine which replaces a small region covering each star’s PSF with a tile of random noise representative of the surrounding sky. The sky noise was sampled separately at the four corners of each tile and linearly interpolated throughout, so as to preserve gradients in the local sky background to first order.

Bright nebulosity can be seen in the center of both images, around the location of IRC+10216’s central star. In addition, the FUV image shows a bright, extended (size  $\sim 24'$ ) ring structure which is not seen in the NUV. Very faint NUV emission is, however, present in this region, as revealed via annular averages of the intensity (§3). The ring is seen mostly on the central star’s east side, and is surrounded on the outside by rather faint, diffuse NUV emission. On the west side several additional diffuse patches of nebulosity can be seen, mostly in the FUV band, forming part of an elongated “tail” structure. Although the ring appears to be roughly circular around the central star’s location, closer inspection shows it be slightly flattened in the easterly direction.

The FUV emission ring represents the interaction of the expanding CSE of IRC+10216 with the local ISM, and the ring’s East-West asymmetry implies that the star is moving roughly eastwards through the local ISM, producing a strong shock at the eastern outer edge of its CSE. The FUV emission is most likely not due to dust scattering of the ambient interstellar radiation field (ISRF): the expected FUV-to-NUV brightness ratio in this case is  $\sim 2.4$  (since the ISRF and dust scattering opacity at NUV wavelengths is, respectively, only about a factor 1.6 and 1.5 lower than in the FUV (Mezger et al. 1982, Whittet 1992)) whereas the observed value is  $\sim 6$ . Martin et al. (2007) consider several possible mechanisms for the FUV emission in Mira, whose wind is also known to be interacting with the ISM, and conclude that the collisional excitation of H<sub>2</sub> by hot electrons in shocked gas is the best candidate for the FUV emission since it produces no detectable counterpart in the NUV band. The same mechanism may be the dominant contributor to the FUV ring emission

in IRC+10216 as well, however a detailed model of H<sub>2</sub> excitation processes is needed to properly address this issue. This exercise is outside the scope of this Letter, and will be addressed in a follow-up paper (see §3, Sahai & Chronopoulos 2010).

Thus the FUV ring around IRC+10216 represents the front resulting from the shocked stellar wind (i.e., the astrosheath); the outer edge of this ring corresponds to the astropause, and the inner edge to the termination shock (see Fig. 2d, Ueta 2008). The region interior to the latter consists of the unshocked, freely-streaming stellar wind; the innermost part of this region is seen in both the NUV and FUV images around the central star’s location due to the scattering of ambient Galactic starlight from dust in the wind. The patchy elongated astrotail shows features which likely correspond to the vortices shed by the shock in the star’s wake, seen in the numerical simulations of a mass-losing AGB star moving through the ISM (Wareing et al. 2007). The diffuse NUV emission around the FUV ring emission most likely represents emission from interstellar material around the astropause.

### 3. The Astropause, Astrosheath and Bowshock

We have measured the astropause radius in different directions from the central star, using radial intensity cuts from the central star location at different position angles. Since the emission from the ring (the astrosheath) is rather faint, we have averaged the intensity over six 30° wedges spanning the eastern limb. These cuts (Fig. 2) show that the radius of the shock varies across the limb, reaching a minimum radius roughly in the eastward direction, as expected from ram pressure considerations due to the (inferred) eastward motion of IRC+10216. We have fit model radial intensities derived from a limb-brightened spherical shell to the FUV radial brightness profiles (assuming the surface brightness to be proportional to the column density) at each *PA* (position angle, measured from north, towards east), and extracted the astrosheath’s inner and outer radii ( $R_1$  and  $R_c$ , using the nomenclature in Fig. 1 of Weaver et al. 1977). A two-piece inverse-square density profile is assumed in our model, one for  $160'' \lesssim r < R_1$  (where the FUV and NUV intensity is well fitted by a  $r^{-\alpha}$  power-law, with  $\alpha$  close to unity, implying optically-thin scattering of Galactic starlight by dust in a stellar wind characterized by a constant  $\dot{M}$  at a constant expansion velocity), and the other for  $R_c > r > R_1$ , with a jump in density at  $r = R_1$ . We cannot derive absolute values of the

densities from our modelling since the proportionality factor between the brightness and the column density is purely phenomenological; furthermore, since the emission mechanisms in the two regions are different, the value of the derived density jump is not physical. The values of  $R_1$  and  $R_c$  which we derive are not sensitive to the assumed density profile within the astrosheath; e.g., a model with a constant density returns very similar values, however the chi-square values of the fits in this case are somewhat poorer. The model fits provide values of  $(R_1, R_c)$  in arcseconds as follows: (580,650), (520,600), (500,590), (500,600), (530,620), (600,700) for the cuts at  $PA = 15^\circ, 45^\circ, 75^\circ, 105^\circ, 135^\circ,$  and  $165^\circ$ .

We note the presence of an FUV emission “plateau” feature that can be seen for about  $100''$  beyond the main peak at  $r = R_c$ , i.e. up to  $r = R_2 \sim 670''$ , in a radial cut of the FUV intensity averaged over a  $30^\circ$  wedge around  $PA = 90^\circ$  (Fig. 3a). This very faint feature can also be seen in the  $30^\circ$ -wide easterly cuts, i.e. at  $PA = 75^\circ$  and  $105^\circ$  (Fig. 2), and directly in the FUV image (Fig. 3b). The presence of this sharp outer edge indicates a pile-up of gas just outside the astropause, and probably represents the bowshock interface separating the shocked and unshocked ISM – the stellar wind material is moving supersonically in the ISM. The post-shock temperature in the bowshock region is expected to be high, about  $(3/16k) \bar{\mu} V_*^2 \sim 10^5 \text{K}$  (assuming a strong shock, where the stellar velocity relative to the ISM,  $V_* = 91 \text{ km s}^{-1}$ , § 4), where  $\bar{\mu} \sim 10^{-24} \text{ g}$  is the mean mass per particle for fully ionized gas. The emission in this region is most likely dominated by emission from hot gas (i.e., a combination of continuous and line emission).

The NUV radial intensity shows a sharp rise just outside the astropause, and then a drop at the bowshock interface, but not to zero: it extends to radii well beyond the bowshock, i.e., up to  $\gtrsim 1000''$ , indicating that the ISM is being heated and/or excited upstream of the bowshock. We will investigate this phenomenon and possible NUV emission mechanisms (e.g., continuous emission from hot gas, line emission from the excited products of ISM ions charge-exchanging with energetic neutrals from the stellar wind) in a follow-up paper (Sahai & Chronopoulos 2010, in prep). Here, we merely note that an analogous situation is found for the heliosphere, where heating and compression of the local ISM (LISM) occurs upstream of the bowshock by charge exchange between secondary H atoms in the solar wind and protons from the LISM plasma (Izmodenov 2004). We also note that at the termination shock,  $R_1$ , the NUV intensity shows an abrupt departure (upwards) from its power-law decrease seen at

smaller radii (the latter results from dust scattering in the unshocked wind, see § 4), implying that there are additional emission mechanisms operational in the astrosheath region than just H<sub>2</sub> line emission (which only contributes in the FUV band).

#### 4. IRC+10216’s Motion through the ISM, Mass-Loss Duration and Circumstellar Mass

We estimate the star’s velocity  $V_*$  through the surrounding ISM using the relationship between  $l_1$ , the distance of the termination shock from the star along the astropause’s symmetry axis (i.e., the termination-shock standoff distance), and  $V_*(\text{km s}^{-1}) = 10 V_{*,6}$  (Eqn. 1 of van Buren & McCray 1988):

$$l_1(\text{cm}) = 1.74 \times 10^{19} (\dot{M}_{*,-6} V_{w,8} / \bar{\mu}_H n_{\text{ISM}})^{1/2} V_{*,6}^{-1} \quad (1)$$

where  $\dot{M}_{*,-6}$  is the stellar mass-loss rate in units of  $10^{-6} M_\odot \text{ yr}^{-1}$ ,  $V_{w,8}$  is the wind velocity in units of  $10^3 \text{ km s}^{-1}$ ,  $\bar{\mu}_H$  is the dimensionless mean molecular mass per H atom, and  $n_{\text{ISM}}$  is the ISM number density in  $\text{cm}^{-3}$ .

Given the strong asymmetry between the eastern and western hemispheres, we first make the simplifying assumption that the astropause’s symmetry axis lies in the sky-plane, i.e., the inclination angle,  $\phi = 90^\circ$ . We find  $l_1 = R_1 = 8.6 \times 10^{17} \text{ cm}$ , using the value of  $R_1 = 478''$  as derived from the easterly cut (shown in Fig. 3). Substituting this value of  $l_1$  in Eqn. 1, with  $\dot{M}_{*,-6} = 20$ ,  $V_{w,8} = 0.014$ ,  $\bar{\mu}_H = 1.33$  (for an 89/11 mixture of hydrogen/helium), and  $n_{\text{ISM}} = 1$ , we get  $V_* = 91 \text{ km s}^{-1}$ . Note that the value of  $V_*$  (i) does not depend on the poorly known distance,  $D$ , to IRC+10216, since both  $l_1$  and  $\dot{M}_{*,-6}^{1/2}$  scale linearly with  $D$ , and (ii) depends only weakly on the uncertain value of the ISM density at IRC+10216’s location.

In order to estimate the inclination angle accurately, we will need to fit a 3-D model of a paraboloidal-shaped emitting astrosheath to the observed emission, which is outside the scope of this Letter. Mac Low et al.’s (1991: MLetal91) paraboloidal bowshock models for various inclination angles (their Fig. 5) show that as  $\phi$  becomes *smaller*, the ratio of the radial distance between the star and the apex of the projected emission paraboloid, to the (unprojected) standoff distance, becomes *larger*. A visual comparison of IRC+10216’s FUV emission morphology (Fig. 1) with the surface brightness countours in Fig. 5 of MLetal91,

indicate that  $\phi$  could be small,  $\sim 30^\circ$ , in which case our measured value of  $R_1$  is larger than  $l_1$  by a significant factor. We speculate that this factor may be as large as  $\sim 1.5 - 2$ , by comparing the length of the (unprojected) standoff distance vector, to the distance between the star and the apex as defined by the emission contours for  $\phi = 30^\circ$  and  $90^\circ$  in Fig. 5 of MLetal91. Thus the value of  $V_*$  may be as high as  $\sim 160 \text{ km s}^{-1}$ .

The FUV emission traces the spherical AGB stellar wind to a much larger distance from the star than previous measurements ( $200''$ , Leão et al. 2006). For example, the radial extent of the astropause along directions orthogonal to the direction of motion of the central star, i.e., at positions angles,  $PA = 0^\circ$  and  $180^\circ$ , is  $700''$  ( $84,000 \text{ AU}$  at  $D = 120 \text{ pc}$ ). Hence, we can use the astropause size to substantially revise (upwards) previous estimates of the duration,  $P$ , of heavy mass-loss in IRC+10216 ( $8000 \text{ yr}$ , Leão et al. 2006). We estimate  $P$  by deriving expansion time-scales ( $P_u, P_s$ ) for the unshocked and shocked wind regions separately;  $P_u = 19,480 \text{ yr}$  from the ratio of the termination shock radius ( $478''$ ) to  $V_w$ , and  $P_s = 49,740 \text{ yr}$  from the ratio of the astrosheath width ( $102''$ ) along the symmetry axis (since the velocity vectors are radial along this axis) to an average velocity for this region,  $\bar{V}_s = 1.17 \text{ km s}^{-1}$ . We take  $\bar{V}_s = V_s/2$ , where  $V_s = V_w (\gamma - 1)/(\gamma + 1) = V_w/6 = 2.33 \text{ km s}^{-1}$ , is the velocity in the astrosheath just beyond the termination shock, with  $\gamma = 7/5$  for diatomic gas, and assuming the latter to be adiabatic. The actual value of  $V_s$  should be less than the adiabatic value, since the astrosheath appears to have cooled to some degree (the astrosheath's average width of  $100''$ , or  $1.8 \times 10^{17} \text{ cm}$ , is smaller than the adiabatic value,  $\approx 0.47 l_1 = 4 \times 10^{17}$  (Eqn. 2, Van Buren & McCray 1988)). Furthermore, once a complete balance has been established between the ram pressures of the stellar wind and the ISM, the leading edge of the astropause remains a fixed distance ahead of the moving star (Weaver et al. 1977). Hence,  $P = P_u + P_s = 69,220 \text{ yr}$  is a lower limit, and we conclude that IRC+10216 has been undergoing mass-loss for at least  $69,000$  years, and the total CSE mass is  $> 1.4 M_\odot$ .

In summary, the GALEX images of IRC+10216 show an unprecedented detailed picture of the interaction of the wind from an AGB star with the ISM, due to its motion in the latter, allowing us to identify all the important structural features expected from theoretical models of such interactions. This interaction process has been observed in the past for other AGB stars (e.g., R Hya: Ueta et al. 2006, Mira: Martin et al. 2007). It is noteworthy that the shock structure on the east side of IRC+10216 is relatively smooth and well-defined, and does

not show the large-scale instabilities (of the order of the standoff distance) which Blondin & Koerwer (1998) predict for stars with slow, dense winds moving relative to the ISM at high speeds (of order  $60 \text{ km s}^{-1}$ ). Our study provides valuable new data for understanding the CSE-ISM interaction, especially since the mass-loss rate in IRC+10216 is about 2 orders of magnitude greater than in R Hya and Mira. New hydrodynamic simulations of stellar wind-ISM interactions (such as, e.g., by Wareing, Zijlstra & O’Brien 2007) to explore the high mass-loss regime represented by IRC+10216’s stellar wind should be carried out.

We thank Drs. D. van Buren, M. Mac Low, T. Ueta, C. Wareing and H.-R. Müller for helpful discussions.

## REFERENCES

- Blondin, J. M., & Koerwer, J. F. 1998, *New Astronomy*, 3, 571
- Crosas, M., & Menten, K. M. 1997, *ApJ*, 483, 913
- Groenewegen, M. A. T., van der Veen, W. E. C. J., & Matthews, H. E. 1998, *A&A*, 338, 491
- Izmodenov, V. V. 2004, *The Sun and the Heliosphere as an Integrated System*, *Astr. & Sp.Sc.Lib.*, 317, 23
- Leão, I. C., de Laverny, P., Mékarnia, D., de Medeiros, J. R., & Vandame, B. 2006, *A&A*, 455, 187
- Mac Low, M.-M., van Buren, D., Wood, D. O. S., & Churchwell, E. 1991, *ApJ*, 369, 395
- Martin, D. C., et al. 2007, *Nature*, 448, 780
- Mauron, N., & Huggins, P. J. 2000, *A&A*, 359, 707
- Mezger, P. G., Mathis, J. S., & Panagia, N. 1982, *A&A*, 105, 372
- Morrissey, P., et al. 2005, *ApJ*, 619, L7
- Sahai, R. 2009, *Asymmetrical Planetary Nebulae IV*, conference proc., I.A.C. electronic publication 2009 (<http://www.iac.es/proyecto/apn4/pages/proceedings.php>), pp. 421

Ueta, T. 2008, ApJ, 687, L33

Ueta, T., et al. 2008, PASJ, 60, 407

van Buren, D., & McCray, R. 1988, ApJ, 329, L93

Wareing, C. J., Zijlstra, A. A., & O'Brien, T. J. 2007, ApJ, 660, L129

Weaver, R., McCray, R., Castor, J., Shapiro, P., & Moore, R. 1977, ApJ, 218, 377

Whittet, D. C. B. 1992, Dust in the Galactic Environment, Institute of Physics Publishing,  
p.67

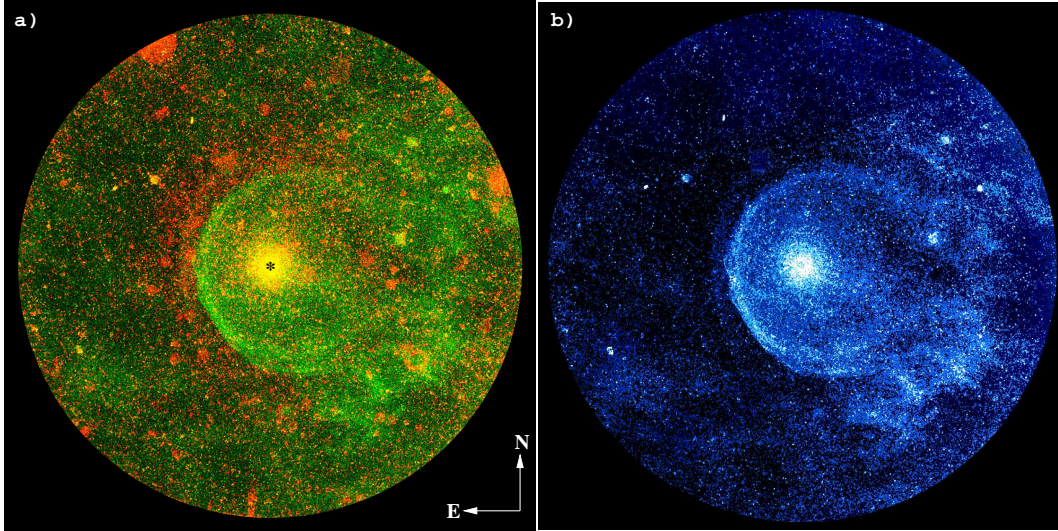


Fig. 1.— (a) Composite [NUV (*red*) & FUV (*green*)] GALEX image of IRC+10216 (the circular field-of-view (FOV) has a diameter of  $61.6' \times 61.6'$ ); the NUV (FUV) image was boxcar-smoothed using a  $3 \times 3$  ( $2 \times 2$ ) pixel box, and displayed using a linear (square-root) stretch. The location of the central star is indicated by a  $\star$ ; the bright round red patches and streaks at the edges of the NUV image are due to bright stars which could not be removed, and detector edge artifacts. (b) The FUV image (same FOV as in a), which is less affected by bright star residuals and artifacts, boxcar-smoothed using a  $3 \times 3$  pixel box, and displayed using a linear stretch (in false color), to clearly show the detailed structure of the astropause and its tail.

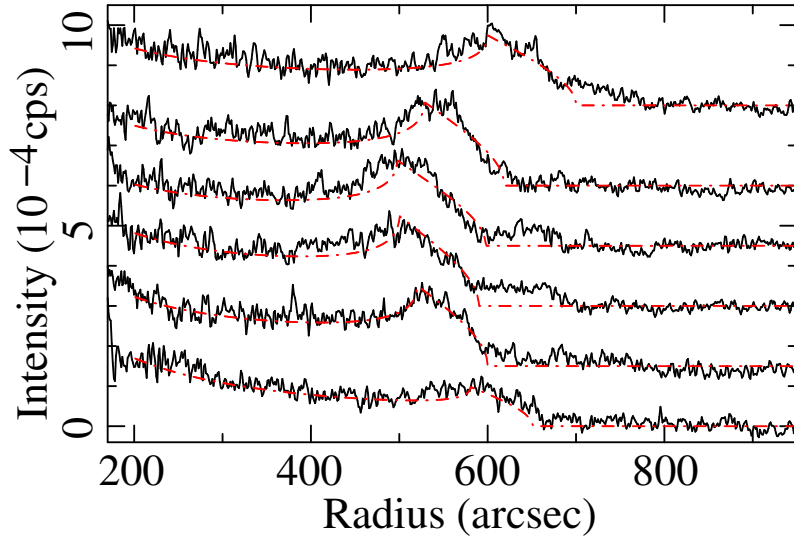


Fig. 2.— Cuts (solid black curves) and models (dash-dot red curves) of the radial intensity averaged over each of six  $30^\circ$  angular wedges on the eastern limb of the FUV emission around IRC+10216; the intensity cuts have been shifted vertically by constant offsets for clarity. The cut  $PAs$  and offsets are (from bottom to top):  $15^\circ(0.0)$ ,  $45^\circ(1.5 \times 10^{-4})$ ,  $75^\circ(3.0 \times 10^{-4})$ ,  $105^\circ(4.5 \times 10^{-4})$ ,  $135^\circ(6.0 \times 10^{-4})$ , and  $165^\circ(8.0 \times 10^{-4})$ . Intensity units are in  $10^{-4}$  cps/pixel, implying a flux of  $1.4 \times 10^{-19}$  erg s $^{-1}$  cm $^{-2}$  Å $^{-1}$  per  $1.5'' \times 1.5''$  pixel.

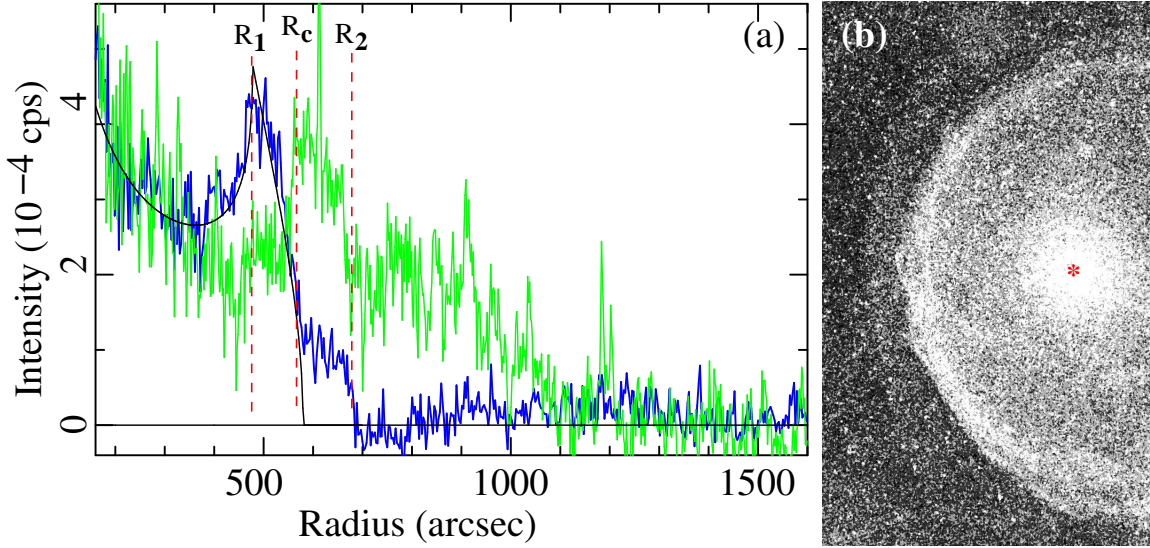


Fig. 3.— (a) Cuts of the the NUV (*green*) and FUV (*blue*) radial intensities obtained by averaging over a  $30^\circ$  wedge around  $PA = 90^\circ$ . A model fit to the FUV intensity, of a limb-brightened shell (*black*), as well as approximate locations of the termination shock ( $R_1$ ), the astropause ( $R_c$ ) and the bowshock ( $R_2$ ), are also shown. The FUV intensity (units as in Fig. 2) has been scaled up by a factor 2. Intensity units for the NUV are in  $10^{-4}$  cps/pixel, implying a flux of  $2.06 \times 10^{-20}$  erg s $^{-1}$  cm $^{-2}$  Å $^{-1}$  per  $1.5'' \times 1.5''$  pixel. (b) Part of the FUV emission around IRC+10216 (box size is  $17.5' \times 29'$ ; orientation, smoothing and stretch as in Fig. 1). The location of the central star is indicated by a  $\star$ .